

EVOLUTION OF MEAN AND FLUCTUATING VELOCITY COMPONENTS IN THE LAMINAR-TURBULENT TRANSITION OF SPHERICAL COUETTE FLOW

Koichi Nakabayashi,^{1*} Zhiming Zheng,² and Yoichi Tsuchida¹

¹Nagoya Institute of Technology, Gokiso-cho, Showa-ku, Nagoya 466-8555, Japan

²Sakai Factory, Daikin Co., Ltd., 1304 Kanaoka-cho, Sakai 591-8511, Japan

*Corresponding author: Koichi Nakabayashi, nakabaya@cfm.mech.nitech.ac.jp

Abstract

In the laminar-turbulent transition of spherical Couette flow with only the inner sphere rotating in the case of gap ratio 0.14, we have studied experimentally the evolution of mean and fluctuating velocities at two meridian angles, $\theta = 60^\circ$ and 90° (the equator). Logarithmic laws have been obtained on mean azimuthal velocity profiles in the turbulent boundary layer near the outer-sphere wall for $\theta = 60^\circ$ and 90° . For a reduced Reynolds number, $R^* = 1.2$, the phase of a fluctuating velocity component in the main-flow direction advances radially from the outer to the inner sphere at $\theta = 90^\circ$, but delays radially at $\theta = 60^\circ$. When R^* is 4.2 and 6.0, the phase slightly advances radially inward at $\theta = 90^\circ$, but does not change so much radially at $\theta = 60^\circ$. The phase-averaged profile of fluctuating velocity in the presence of spiral Taylor-Görtler (TG) vortices differs from that in the presence of traveling azimuthal waves. Spiral TG vortices make the amplitude of fluctuating velocity large in the central part of the gap. But traveling azimuthal waves make it large somewhat near the inner sphere.

Introduction

We have studied characteristics of mean and fluctuating velocities in the laminar-turbulent transition of spherical Couette flow (SCF) between a rotating inner and a fixed outer sphere with the gap ratio $\beta = 0.14$ where the Taylor vortex occurs near the equator. In our early study [1], we identified spiral TG vortices, traveling azimuthal waves on toroidal and spiral TG vortices, and shear waves within the Ekman-type secondary flow, and also clarified their wavenumbers, fundamental frequencies and rotation frequencies. Further, we clarified the Reynolds-number-dependence of profiles of the time-averaged velocity (mean velocity) and turbulence intensity (rms value) for an azimuthal velocity component in the gap at $\theta = 80^\circ$ and 90° where the TG vortices develop.

However, the relationship between the TG-vortex structure and the mean and fluctuating velocities has not been investigated. The mean velocity profile near the equator varies largely with the location of inflow and outflow boundaries of the TG vortices which moves in the meridian direction with increasing Reynolds number. On the other hand, since the fluctuating velocity corresponds to periodic or unperiodic fluctuating motion of vortices, it is important to investigate the relationship between the vortex structure and the velocity fluctuation.

Accordingly, we measured the velocities both at $\theta = 60^\circ$

where the Ekman-type secondary flow is always located and at $\theta = 90^\circ$ where the toroidal TG vortex occurs; and we investigated the temporal phase difference and phase-averaged fluctuating velocity in the main-flow direction. We also consider the law of the wall for the mean azimuthal velocity component near the outer sphere.

Experimental Setup And Measurement Method

The experimental apparatus is the same as that in our early study [1]. The gap ratio, $\beta = (R_2 - R_1)/R_1$, is 0.14, where R_1 and R_2 are the radii of the inner and outer spheres. The Reynolds number, $Re = U_0 R_1 / \nu$ ($U_0 = 2\pi R_1 f_0$), is quasi-statically increased from zero, where f_0 is the rotation frequency of the inner sphere; U_0 is the peripheral speed at the equator of the inner sphere; and ν is the kinematic viscosity. In the present paper, a reduced Reynolds number, $R^* = Re/Re_c$, is used, where Re_c is the critical Reynolds number of the Taylor instability and is 880 for $\beta = 0.14$ [1].

The measuring system of velocities is the same as that in our early study [1]. Instantaneous velocities in the main-flow direction in the plane perpendicular to the radial coordinate r were measured at any dimensionless distance from the inner sphere, defined as $\eta = (r - R_1)/(R_2 - R_1)$, at $\theta = 60^\circ$ and 90° by a hot-wire anemometer, and were decomposed into mean and

fluctuating velocities, U_m and $u_m(t)$, respectively (t is time). Mean azimuthal and meridian velocity components, U and W , respectively, were obtained from U_m as $U=U_m \cos \alpha$ and $W=U_m \sin \alpha$, where α ($=\tan^{-1}(W/U)$) is the time-averaged angle of the main flow measured from the azimuthal direction on the plane perpendicular to r .

Experimental Results

1. Mean velocity profiles in the gap

Figs. 1(a) and (b) show dimensionless mean velocity profiles of azimuthal and meridian components, U^* ($=U/U_0$) and W^* ($=W/U_0$), respectively, in the gap at $\theta=60^\circ$. Profiles at $R^*=0.94$ show analytical results for the laminar basic flow obtained by Nakabayashi [2]. The experimental results of W^* at $R^*=1.2$ are close to the analytical ones. With increasing R^* , the value of U^* decreases on the inner-sphere side and increases on the outer-sphere side, so that the gradient of profile U^* varies gradually from negative to positive in the center of the gap. This is because, with increasing R^* , W^* becomes large in magnitude near both spheres, i. e., the circulation of the Ekman-type secondary flow becomes strong. For $R^*\geq 20$, the flow is chaotic and the turbulence activity becomes strong [1], so that the profile of U^* tends to be flat.

2. Law of the wall near the outer sphere

We consider the law of the wall for U^* near the fixed outer sphere, comparing with the law of the wall for turbulent plane boundary layer flow (TPBLF) [3], circular Couette flow with only the inner cylinder rotating (CCF) [4], and turbulent shear flow around a rotating cylinder in a quiescent fluid (TSFRC-QF) [5] and that in a uniform flow (TSFRC-UF) [6], respectively.

Nakamura et al. [5, 6] obtained the following logarithmic law for the mean azimuthal velocity component U near the rotating cylinder wall of TSFRC-QF and that of TSFRC-UF, taking into account the effect of streamline curvature.

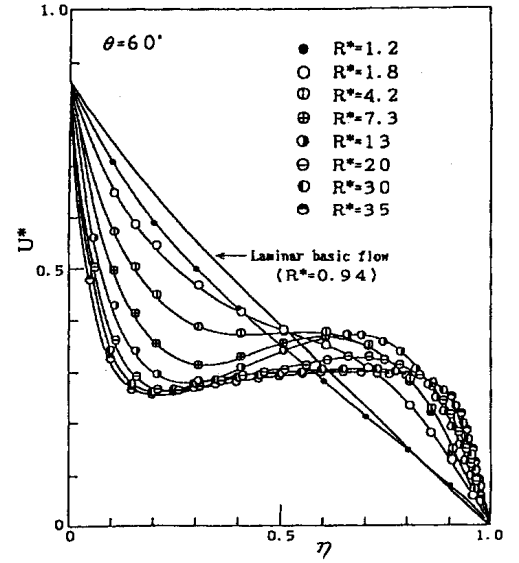
$$U^+ = (1/0.55) \ln y^+ + 9.8 \quad (\text{TSFRC-QF}), \quad (1)$$

$$U^+ = (1/0.65) \ln y^+ + 6.5 \quad (\text{TSFRC-UF}), \quad (2)$$

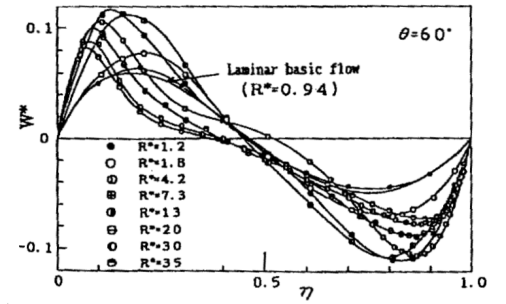
$$\begin{aligned} U^+ &= (U_w/a - U/r) / (U_\tau/a), \\ y^+ &= \{a(1 - a^2/r^2)/2\} U_\tau / \nu. \end{aligned} \quad (3a,b)$$

U_w is the peripheral speed of the rotating cylinder; a is the cylinder radius; r is the radial coordinate in the cylindrical coordinate system; and U_τ is the friction velocity.

In the present study, following Nakamura et al. [5, 6], we consider the law of the wall for U near the outer sphere. We can obtain the next equation near the outer-sphere wall by imposing the axisymmetric condition and neglecting the inertia terms in the Reynolds equation.



(a) Azimuthal velocity component U^* .



(b) Meridian velocity component W^* .

Figure 1: Mean velocity profiles at $\theta=60^\circ$.

$$r^3 \tau_{r\phi} = \text{const.} \quad (\tau_{r\phi} = \mu r \partial(U/r) / \partial r - \rho uv), \quad (4)$$

where u and v are instantaneous azimuthal and radial velocity components; and μ and ρ are the dynamic viscosity and density of the fluid.

In the viscous sub-layer where the Reynolds shear stress $-\rho uv$ can be neglected, Eq. (4) becomes

$$r^3 [\mu r \partial(U/r) / \partial r] = \text{const.} \quad (5)$$

By integrating Eq. (5) and using the no-slip condition at the outer sphere, we can obtain the following linear law.

$$U^+ = y^+, \quad (6)$$

$$U^+ = (U/r) / (U_\tau / R_2), \quad (7a,b)$$

$$y^+ = \{R_2(R_2^3/r^3 - 1)/3\} U_\tau / \nu, \quad (7a,b)$$

$$U_\tau = \{(-\tau_0) / \rho\}^{0.5}. \quad (8)$$

$\{R_2(R_2^3/r^3 - 1)/3\}$ is a proper length scale, as seen from Eq. (7b). τ_0 ($\tau_0 < 0$) is the wall shear stress at the outer sphere.

In the fully turbulent region, Eq. (5) can be rewritten as follows by using the eddy viscosity ν_T .

$$r^3 [\rho \nu_T r \partial(U/r) / \partial r] = R_2^3 \tau_0, \quad (9)$$

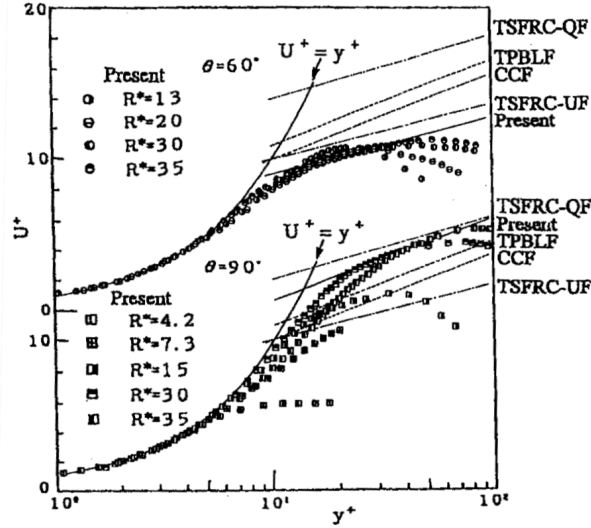


Figure 2: Logarithmic representation of the mean azimuthal velocity profile near the outer sphere at $\theta=60^\circ$ and 90° .

where v_T is given by

$$v_T = \kappa U_\tau \{R_2(R_2^3/r^3 - 1)/3\}. \quad (10)$$

By substituting Eq. (10) into Eq. (9) and then integrating Eq. (9), we obtain

$$U^+ = (1/\kappa) \ln y^+ + C, \quad (11)$$

where κ is Karman constant and C is an additive constant.

Present experimental data at $\theta=90^\circ$ and 60° for $4.2 \leq R^* \leq 35$ are shown in Fig. 2. The present results agree with the linear law for $y^+ < 5$. In the fully turbulent flow for $R^* \geq 20$, the following logarithmic law holds.

$$U^+ = (1/0.63) \ln y^+ + 5.3 \quad \text{at } \theta=60^\circ. \quad (12)$$

$$U^+ = (1/0.41) \ln y^+ + 7.1 \quad \text{at } \theta=90^\circ. \quad (13)$$

The logarithmic law at $\theta=60^\circ$ virtually agrees with that for TSFRC-UF [6], while that at $\theta=90^\circ$ virtually agrees with that for TSFRC-QF [5]. In comparison with CCF [4], U^+ at $\theta=60^\circ$ is smaller than that for CCF, while U^+ at $\theta=90^\circ$ is larger than the latter. Therefore, the effect of wall curvature in the meridian direction appears strongly in the present results.

3. Temporal phase difference and phase-averaged fluctuating velocity in the gap

The temporal phase difference Γ between two sets of time-series records, $u_m(t)$ at $\eta=0.9$ and $u_m(t)$ at any η , at the same meridian angle θ was accurately obtained from the two-point correlation coefficient,

$$R_{12}(\tau) = \frac{(u_m(t))_{0.9} (u_m(t-\tau))_\eta}{\{(u_m)_{0.9}^2 (u_m)_\eta^2\}^{0.5}}, \quad (14)$$

where τ is a time lag and $R_{12}(\tau = \Gamma) = 1$.

Fig. 3 shows the variation of Γ in the radial direction. For $R^*=1.2$, the velocity fluctuation is caused only by spiral TG vortices. The phase of the fluctuation advances radially from the

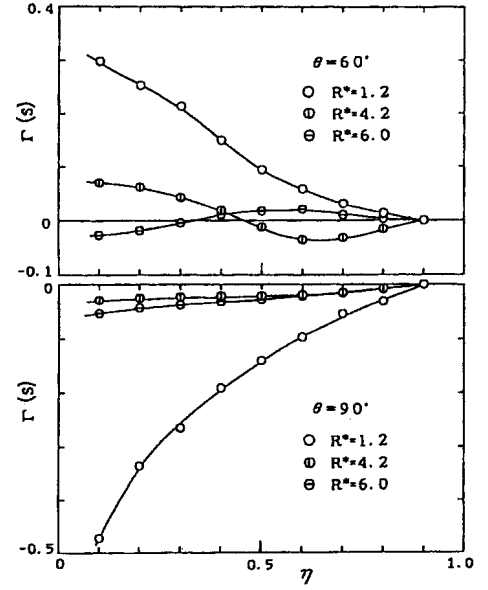


Figure 3: Temporal phase difference Γ of the fluctuating velocity in the main-flow direction at $\theta=60^\circ$ and 90° .

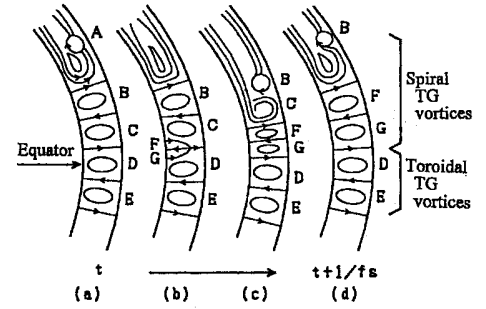


Figure 4: Temporal evolution of toroidal and spiral TG vortices at the meridian cross-section ($R^*=1.2$).

outer to the inner sphere at $\theta=90^\circ$, while it delays radially at $\theta=60^\circ$. For $R^*=4.2$, on the other hand, the fluctuation is by both spiral TG vortices and traveling azimuthal waves on TG vortices. The phase slightly advances from the outer to the inner sphere at $\theta=90^\circ$, slightly advancing near the outer sphere and then delaying radially inward at $\theta=60^\circ$. For $R^*=6.0$, the fluctuation is only caused by traveling azimuthal waves on toroidal TG vortices at the equator. The phase slightly advances radially from the outer sphere at $\theta=90^\circ$, but slightly delays near the outer sphere and then advances radially inward at $\theta=60^\circ$.

To consider the possible reason for the variation of Γ for $R^*=1.2$ and 6.0 , we observed the meridian cross-section of the flow. Fig. 4 gives a schematic of the temporal evolution of toroidal and spiral TG vortices at the meridian cross-section for

$R^*=1.2$, where D and E are toroidal TG vortex cells, and A, B, C, F and G are spiral ones. In Fig. 4(b), a new pair of spiral TG vortex cells, F and G, appear in the outflow boundary at $\theta \cong 85^\circ$ between D and C. Then, they develop from the inner to the outer sphere (Fig. 4(c)). This is the reason that the phase of velocity fluctuation advances more in closer proximity to the inner sphere at $\theta=90^\circ$. With the appearance of the spiral TG vortex cells, F and G, spiral TG vortex cells B and C begin to collapse at $\theta \cong 70^\circ$ (Fig.4(d)). The tail of the spiral TG vortex cell C passes through on the outer-sphere side at $\theta=60^\circ$. This is the reason that the phase of fluctuation advances more in closer proximity to the outer sphere at $\theta=60^\circ$. Fig. 5 presents a schematic of the oscillation of inflow and outflow boundaries of toroidal TG vortices for $R^*=6.0$. The outflow boundaries at $\theta \cong 80^\circ$ and 100° of the toroidal TG vortex cell oscillate approximately parallel to the equator, but the inflow boundary at $\theta=90^\circ$ oscillates with a fixed fulcrum at the outer sphere. This is the reason that the phase of fluctuation advances more in closer proximity to the inner sphere at $\theta=90^\circ$.

Fig. 6 shows the temporal variation of the dimensionless phase-averaged fluctuating velocity component $\langle u_m^*(t^*) \rangle$ ($=\langle u_m(t^*) \rangle / U_0$) in the main-flow direction for different values of η . At $\theta=60^\circ$ for $R^*=1.2$, the velocity fluctuation has a large amplitude near $\eta=0.6-0.7$. This fluctuation is caused by the spiral TG vortex tail which is carried away to the pole as shown in Fig. 4. At $\theta=90^\circ$ for $R^*=6.0$, the velocity fluctuation has the large amplitude on the inner-sphere side from the center of the gap. This is because of the oscillation of the inflow boundary at $\theta=90^\circ$, as seen in Fig. 5.

Conclusions

(1) The profile of the mean azimuthal velocity component at $\theta=60^\circ$ is strongly influenced by the circulation of the Ekman-type secondary flow.

(2) The logarithmic law holds for the mean azimuthal velocity component near the outer sphere, although the velocity vector with azimuthal and meridian components is largely twisted in the log-region.

(3) When the velocity fluctuation is caused only by spiral TG vortices, the phase of the fluctuation advances radially from the outer to the inner sphere at $\theta=90^\circ$, while it delays radially at $\theta=60^\circ$. When the velocity fluctuation is caused by traveling azimuthal waves, the phase slightly advances radially inward at $\theta=90^\circ$, but does not change so much radially at $\theta=60^\circ$.

(4) Spiral TG vortices make the amplitude of fluctuating velocity large in the central part of the gap. But traveling azimuthal waves make it large somewhat near the inner sphere.

References

- [1] Nakabayashi, K., and Tsuchida, Y., 1988, "Spectral study of the laminar-turbulent transition in spherical Couette flow," J. Fluid Mech. 194: 101-132.
- [2] Nakabayashi, K., 1976, "Study on the flow between rotating spheres, 1st report, Theoretical study," Trans. Japan Soc. Mech. Engrs (in Japanese) 42: 1839-1848.
- [3] Cebeci, T., and Smith, A. M. O., 1974, Analysis of Turbulent Boundary Layers, Academic Press, New York, page. 100.
- [4] Smith, G. P., and Townsend, A. A., 1982, "Turbulent Couette flow between concentric cylinders at large Taylor numbers," J. Fluid Mech. 123: 187-217.
- [5] Nakamura, I., Ueki, Y., and Yamashita, S., 1983, "The turbulent shear flow on a rotating cylinder in a quiescent fluid," Trans. Japan Soc. Mech. Engrs (in Japanese) 49: 2230-2235.
- [6] Nakamura, I., Yamashita, S., Watanabe, T., and Sawaki, Y., 1981, "Three-dimensional turbulent boundary layer on a spinning thin cylinder in an axial uniform stream," in Proceeding of the 3rd Symposium on Turbulent Shear Flows, edited by L. J. S. Bradbury, U. C. Davis, California, 2: page 7.

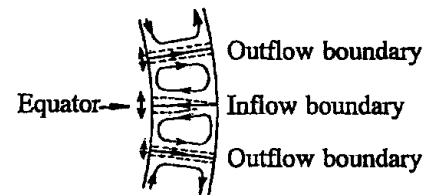
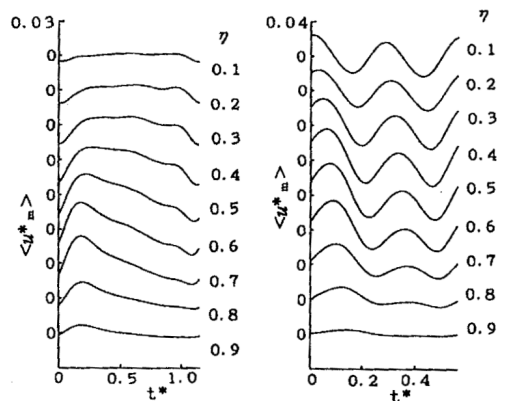


Figure 5: Oscillation of inflow and outflow boundaries of toroidal TG vortices at the meridian cross-section ($R^*=6.0$).



(a) $\theta=60^\circ$ for $R^*=1.2$. (b) $\theta=90^\circ$ for $R^*=6.0$.
Figure 6: Temporal variation of phase-averaged fluctuating velocity in the main-flow direction for different values of η .